Evidence for an Antiferromagnetic Transition in a Zeolite-Supported Cubic Lattice of *F* Centers

V. I. Srdanov,[1] G. D. Stucky,[1] E. Lippmaa,[2] and G. Engelhardt[3]
[1]*Department of Chemistry, University of California, Santa Barbara, California 93106*
[2]*Institute of Chemical Physics and Biophysics, EE0001 Tallinn, Estonia*
[3]*Institute of Chemical Technology I, University of Stuttgart, D-70550 Stuttgart, Germany*
(Received 8 October 1997)

Evidence for a bcc lattice of *F* centers in sodium-electro-sodalite (SES), synthesized by exposing dehydrated sodalite to sodium vapor, is presented. A high electron spin density in SES produces isotropic contact shifts in nuclear magnetic resonance (NMR) spectra of the framework nuclei whose magnitude is a discrete function of local electron density. Strong exchange coupling between unpaired electrons gives rise to an antiferromagnetic phase transition in SES at $T_N = 48 \pm 2$ K, providing the first example of an *s*-electron antiferromagnet. [S0031-9007(98)05448-9]

PACS numbers: 75.30.Hx, 61.72.Ji, 76.60.–k

Magnetic measurements on isolated *F* centers have been extensively pursued in the past, yet little is known about properties of an ensemble of interacting *F* centers. This is because the density of *F* centers in ionic solids seldom exceeds 10^{18} cm^{-3}, where they are still separated by 100 Å on average. Previous attempts to increase *F* center density by exposing ionic solids to visible light and/or thermal neutrons led to a concoction of loosely bound $[F]$ center aggregates, the remaining "unreacted" *F* centers, and colloidal metallic particles. The electron paramagnetic resonance (EPR) studies of such solids have proven difficult to interpret, while NMR measurements are generally not possible for reasons of sensitivity [1]. As we show below, such a restriction does not apply to certain zeolites, where a large density of ionic clusters, analogous to *F* centers in ionic solids, can be formed. These centers were first detected in zeolite *Y* exposed to high energy radiation [2] but were also discovered in zeolites exposed to alkali vapor [3]. The second method produces a much higher density of *F* centers yielding solids with unusual [4] and often controversial [5,6] physical properties. Some conflicting data are, in part, due to the structural complexity of commonly used large-pore zeolites where alkali clusters of various sizes and electric charges can form [7]. In this report, we restrict our attention to a model system consisting of a simple sodalite lattice [8] built of uniform cages that host just one type of ionic cluster. Sodalite cages are present in several important but structurally more complex zeolites, hence, the results are of general interest.

In this Letter, a magnetic study of an ordered zeolite-supported bcc lattice of *F* centers is presented. The particular type of *F* centers consists of an unpaired electron trapped by four equivalent sodium ions forming a Na_4^{3+} ionic cluster [2]. The supporting lattice belongs to the well-known mineral sodalite in which the central cage anion, such as Cl^-, has been replaced by an unpaired electron [9]. Following the common nomenclature, we name this unusual lattice *sodium-electro-sodalite,* abbreviated hereafter as SES. The origin of the *F* center electron wave function in SES coincides with the center of the sodalite cage but a fraction of electron density extends beyond the cage boundaries. This gives rise to a strong exchange coupling between unpaired electrons, which culminates in an antiferromagnetic transition at 48 K. Evidence for this was found in temperature-dependent NMR, EPR, and static susceptibility measurements presented below. We emphasize that unpaired electrons in Na_4^{3+} centers have predominantly an *s* character [10], therefore making SES, to the best of our knowledge, the first example of an *s*-electron antiferromagnet.

The sodalite framework is built of regularly alternating oxygen-sharing AlO_4 and SiO_4 tetrahedra with Si and Al atoms occupying apexes of a truncated octahedron (see Fig. 1), often called the sodalite cage. For a typical sodalite, these cages contain four alkali cations surrounding a negative central anion in a tetrahedral geometry. Defect cages with a missing central anion are potential nests for Na_4^{3+} centers that easily form in halogen sodalites exposed to high energy radiation [11]. In this study, such *F* centers were prepared via sodium doping of a particular sodalite [12], hereafter called sodium-sodalite, whose cages contain only three sodium cations and no central anion. Sodium-sodalite, like other zeolites, readily absorbs water but is also capable of absorbing and ionizing an excess sodium atom. When exposed to sodium vapor, white sodium-sodalite turns blue, then purple, and eventually black [13]. The color change is due to formation of Na_4^{3+} clusters made of three existing sodium ions and an excess sodium atom absorbed by the sodalite cage. A recent structural study showed that exposure of sodium-sodalite to sodium vapor at 650 K proceeds by inclusion of just one sodium atom per sodalite cage: $Na_6(AlSiO_4)_6 + 2Na = Na_8(AlSiO_4)_6$. The resulting SES lattice is cubic ($P\bar{4}3n, a_0 = 8.881$ Å) and contains 3×10^{21} unpaired electrons per cm^3 separated from each other by precisely 0.768(2) nm [14]. Face-sharing sodalite cages are stacked in a close-packed bcc

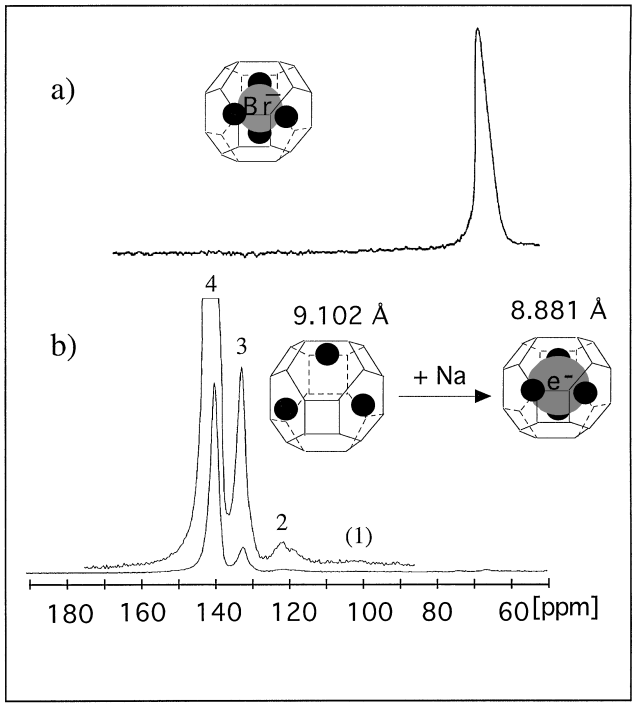

FIG. 1. (a) ^{27}Al MAS NMR spectrum of a typical halogen sodalite. Inset: schematic of sodium-bromo-sodalite cage. Apexes of the truncated octahedron are occupied by regularly alternating aluminum and silicon atoms bridged by an oxygen atom. (b) ^{27}Al MAS NMR spectrum of SES. The observed resonances are labeled according to the number of F centers around an aluminum site. Inset: cage of sodium-sodalite and that of sodium-electro-sodalite (SES), with the corresponding unit cell constants a_0. Note that the sodalite unit cell takes up the volume of two sodalite cages.

superlattice, for unpaired electrons in SES give rise to a bcc spin lattice.

When observed, NMR resonances of paramagnetic solids are always displaced with respect to the resonances in diamagnetic materials of similar kind. For localized electrons, paramagnetic shifts may be due to isotropic Fermi contact interaction and/or dipole pseudocontact interaction. The dipolar shift in cubic SES vanishes because s-like electrons associated with tetrahedral Na_4^{3+} centers have only an isotropic g tensor [10]. This leaves the Fermi contact interaction as the only source of the observed shifts [15] whose magnitude is governed by [16]

$$(\Delta B/B)_{\text{contact}} = -(A_0/g\mu_B\gamma_N)\chi_e(T)\,. \qquad (1)$$

A_0 is the hyperfine coupling constant, μ_B is the Bohr magneton, and γ_N is the nuclear magnetogyric ratio. Magnetic susceptibility $\chi_e(T)$ can be expressed by the Curie-Weiss law $\chi_e(T) = C/(T - \Theta)$, where C is the Curie constant, T is the absolute temperature, and Θ is the Weiss temperature. The absence of strong spinning sidebands in the NMR spectra of SES is consistent with small or vanishing dipolar contribution. We also note that NMR contact shifts should be independent of nuclear properties, since substitution for the hyperfine coupling constant $A_0 = \frac{2}{3}\,\mu_0 g_e \mu_B \gamma_N h|\Psi(0)|^2$ eliminates γ_N from Eq. (1). This statement is strictly true for isotopes of the given element because electron probability density $|\Psi(0)|^2$ depends on the atomic number. Nevertheless, in a special case such as sodalite, practically identical paramagnetic shifts of ^{27}Al and ^{29}Si nuclear resonances are expected, in agreement with experiment [17]. Sodalite belongs to a special case because its framework Si and Al atoms are crystallographically equivalent and nearly isoelectronic.

The sodalite ^{27}Al magic angle spinning (MAS) NMR spectra above 140 K were recorded on a Bruker MSL-400 spectrometer, while the low-temperature data were collected by using a wide bore CXP-360 spectrometer. The ^{23}Na MAS NMR spectra were obtained on a modified GN300 spectrometer. The ^{27}Al NMR spectrum of a cubic sodalite consists of a single resonance, shown in Fig. 1(a), which varies insignificantly (67 ± 6 ppm) within the members of the halogen-sodalite series [18]. As shown in Fig. 1(b), this resonance is shifted to 140 ppm in SES, due mainly to the presence of unpaired electrons. The $\bar{4}$ site symmetry of the framework Al reflects the fact that there are four equivalent sodalite cages around each Al site. Consequently, aluminum nuclei in SES can be exposed to electron density from up to four nearest F centers. This gives rise to four additional resonances whose paramagnetic shifts, assuming noninteracting electrons, should be a linear function of the quantized increase in the local electron density:

$$(\Delta B/B)_{\text{contact}} = C|\Psi_{\text{Al}}(0)|^2 = Cn\rho_F\,. \qquad (2)$$

Here, C is a constant at given temperature, $|\Psi_{\text{Al}}(0)|^2$ is the electron probability density at the aluminum nucleus, n is an integer between 0 and 4, and ρ_F is the electron density contribution from a single F center. Except for surface cages, all aluminum nuclei in fully doped SES are exposed to the same electron density giving rise to the strong resonance at 140 ppm in Fig. 1(b). Aluminum atoms from the surface and undoped sodalite cages are exposed to electron density from either three or two nearest F centers, giving rise to weak resonances at 133 and 120 ppm, respectively. The relative intensities of these resonances indicate that no more than 4% of such cages were present in this particular sample. Because of the large difference in the lattice constants between SES and its precursor, cages with Na_4^{3+} centers tend to bunch during the doping, yielding a large SES surface in a partially doped sample. In such cases, the ^{27}Al spectra contain resonances at 133 and 120 ppm that may be comparable to [17] or stronger [14] in intensity than the one at 140 ppm. Such a sample may also contain an additional broad resonance at around 100 ppm that belongs to the Al atoms exposed to electron density from a single F center. It is interesting to note that aluminum paramagnetic shifts do not increase linearly with the number of the surrounding F centers as would be expected for noninteracting electrons. We attribute such behavior to Coulomb repulsion between localized

electrons that increases nonlinearly with an increase of the local electron density.

In cubic sodalite, there is only one sodium crystallographic site, thus giving rise to a single ^{23}Na NMR resonance at around 0 ppm. By substituting $A_0 = 2.8$ mT for a typical value of sodium hyperfine coupling constant in Na_4^{3+}, the ^{23}Na NMR resonance in SES should be expected at around 10^4 ppm. As in the recent NMR study of sodium-doped zeolite *Y* [19], no such resonance has been found in SES. This is presumably due to a fast electron-mediated spin-lattice relaxation rate that may severely broaden the sodium resonance. Nevertheless, the absence of ^{23}Na resonance at around 0 ppm in Fig. 2(a) confirms that each sodium ion is exposed to a substantial electron density. The sodium Knight shift at 1123 ppm is due to excess metallic sodium at the sodalite surface which can be removed by careful redistillation. In such a sample, the Knight shift resonance is replaced by a weak and temperature-independent sodium resonance at around 50 ppm that quickly vanishes from the NMR spectrum after the sample is exposed to air [see Fig. 2(a)]. The same procedure leaves the ^{27}Al spectrum of SES practically unchanged, showing that Na_4^{3+} centers inside the sodalite crystallites are air resistant. From this, it follows that the temperature-independent 50 ppm resonance, which was also observed in sodium-doped zeolite *Y* [19], belongs to a certain diamagnetic sodium species on the zeolite *surface* that may form during zeolite exposure to sodium vapor.

As shown in Fig. 2(b), the paramagnetic shift of the ^{27}Al NMR resonance of SES increases with lowering temperature, as expected from Eq. (1). This trend persists down to 50 K, where the NMR resonance linewidth begins to increase rapidly while the magnitude of the paramagnetic shift stops increasing. Such behavior indicates change in the electronic structure induced by a magnetic phase transition whose type was established by the magnetic susceptibility measurements shown in Fig. 3. Because of the polycrystalline nature of the sample, strong local fields add to the external magnetic field in a random way, which broadens the NMR resonance below the critical temperature. According to Eq. (1), the magnitude of the paramagnetic shift is linearly proportional to the magnetic susceptibility of unpaired electrons. Indeed, the reciprocal values of the shift as a function of temperature, plotted in Fig. 2(c), can be fitted to the Curie-Weiss law yielding $\Theta = -178 \pm 8$ K. Such a value of Θ implies a strong antiferromagnetic exchange interaction in the paramagnetic phase consistent with the absence of the Na_4^{3+} hyperfine structure in the EPR spectra of SES in Fig. 3(a). The latter are directly compared with the EPR spectra of α, α'-diphenyl-β-pichrylhydrazyl (DPPH), a paramagnetic organic solid widely used as an EPR frequency standard. While both solids suffer from the loss of hyperfine structure due to exchange narrowing, the SES line intensities above 60 K are obviously far from the DPPH Curie behavior. Instead, SES shows almost Pauli-like susceptibility that is also noticeable in the magnetic susceptibility data in Fig. 3(b). It is also evident that SES EPR resonance in Fig. 3 vanishes below 50 K, while an obvious kink appears at that point in the magnetic susceptibility. After correcting for the low-temperature Curie tail caused by uncompensated surface spins, magnetic susceptibility of SES gives a textbook example of an antiferromagnetic phase transition in a polycrystalline sample. From the data shown in the inset of Fig. 3, the maximum in the susceptibility $\chi_{\max}$ was found at 55 ± 2 K and the critical temperature [20] to be $T_N = 48 \pm 2$ K. The estimate of experimental uncertainty in the Néel temperature was based on the temperature interval (1 K) between the measurements and the fact that powder, rather than single crystal, susceptibility was measured. The least-squares fit of integrated EPR intensities to the Curie-Weiss law yields

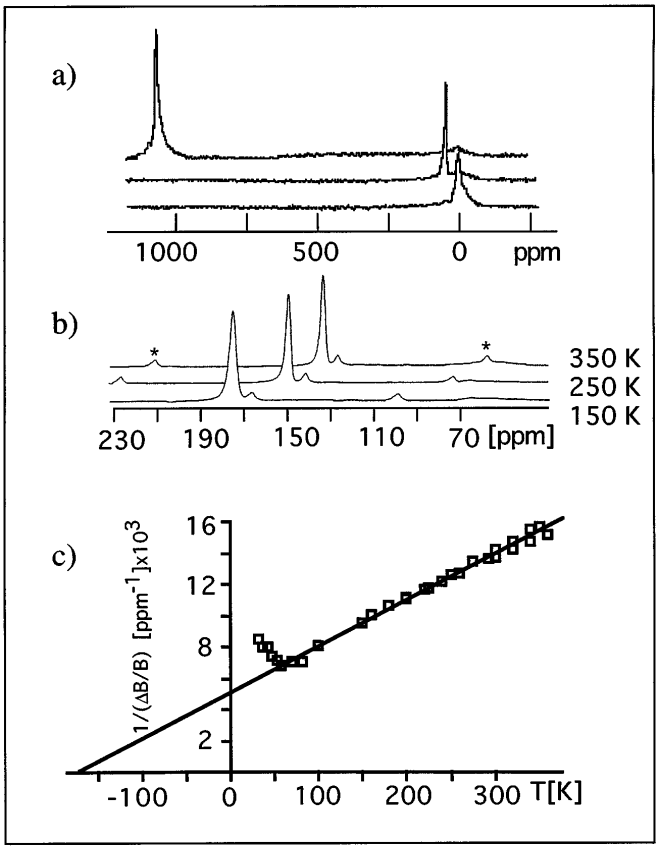

FIG. 2. (a) ^{23}Na MAS NMR spectra of SES with excess of metal sodium at the surface (top), after removal of the metallic layer (middle), and after sample exposure to air (bottom). Note that sodium atoms inside SES cages do not contribute to the above spectra and that Na_4^{3+} centers in sodalite remain stable for many days in air. (b) ^{27}Al MAS NMR spectra of SES at selected temperatures. Spinning sidebands are denoted with an asterisk. (c) Inverse paramagnetic shifts of the main ^{27}Al resonance in SES as a function of temperature. The straight line is the result of the least-squares fit to the Curie-Weiss law in the 60–350 K region. Data between 30 and 160 K are from the static NMR measurements, while those between 160 and 350 K were obtained by using an MAS probe. Measurements from several SES samples were combined.

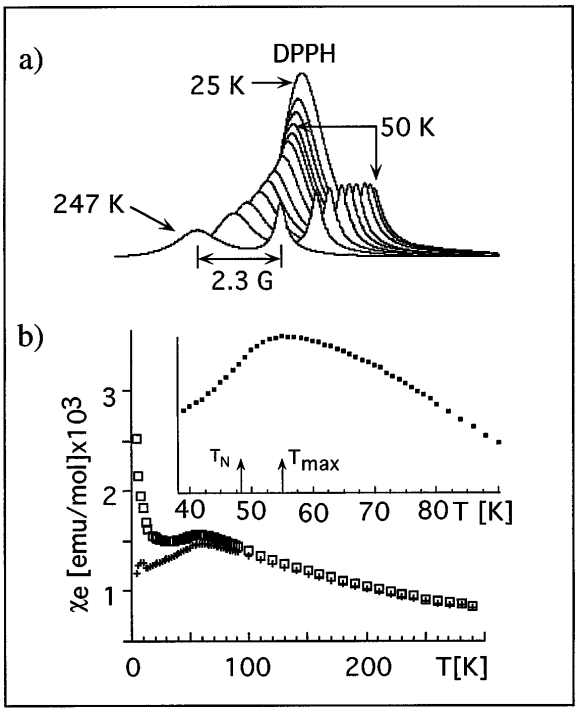

FIG. 3. (a) Temperature-dependent EPR spectra of SES and that of DPPH obtained simultaneously on an X-band ESP-300 Bruker spectrometer equipped with an Oxford 91 000 liquid helium flow cryostat. Both solids have narrow resonances with sufficiently different g values ($g = 2.0014$ for SES) yielding well-resolved signals. The widths (FWHM = 0.67 G for SES) of both resonances do not change significantly in the 60–300 K region allowing for visual comparison of their relative intensities. The SES resonance abruptly disappears below 50 K. (b) Magnetic susceptibility of SES after diamagnetic correction (squares) and after subtraction of the paramagnetic contribution from uncompensated surface spins (crosses). The surface spins constitute ~2% of the total susceptibility at room temperature. Inset: expanded plot of the corrected susceptibility data in the critical region used for determination of $\chi_{\max}$ and T_N. Data were obtained by using a Quantum Design model MDMS-5S SQUID susceptometer.

$\Theta = -190 \pm 10$ K, while the dc magnetic susceptibility data give $\Theta = -210 \pm 5$ K. The latter is the more reliable, given the accuracy of the SQUID method and the ease of the diamagnetic correction by using the sodium-sodalite precursor. Assuming only nearest neighbor interaction, one obtains -4.3 meV for the exchange coupling constant J, from $J = 3k\Theta/2zS(S + 1)$ [21] and $\Theta = -200$ K. This value is clearly an overestimate, given the fact that the Θ/T_N ratio in SES exceeds the maximum theoretical value for a bcc lattice [22], which raises a question about the physical significance of Θ obtained from the least-squares fits to the Curie-Weiss law.

While there is no doubt that SES acquires an antiferromagnetic ground state below 48 K, its picture as a Mott insulator at room temperature is somewhat obscured by the Pauli-like susceptibility behavior. Even though the high electron-spin density places SES near the metal-insulator border, there are no indications of a metallic state at room temperature. This is supported by the existance of a 0.7 eV optical gap in SES [23] and the fact that no dc conductivity has been found in a pressed polycrystalline sample. Perhaps most convincing are the quantized NMR shifts in SES that are clearly inconsistent with itinerant electrons. We also note, at the end, that a metal-insulator dilemma has been present in the theoretical papers concerning SES, among which the calculations of Monnier *et al.* [24] appear closest to our experimental data.

We thank D. Margolese, I. Heinmaa, and M. Feuerstein for help with NMR data acquisition and J. Allen, D. Markgraber, and L. van Wüllen for many valuable discussions. This work was supported by the following agencies: NSF (DMR-9520970), ACS (PRF No. 30230), and ONR. G. E. thanks the Deutsche Forschungsgemeinschaft and the Max-Buchner-Forschungsstiftung for support.

[1] H. Seidel and H. C. Wolf, in *Physics of Color Centers*, edited by W. B. Fowler (Academic, New York, 1968), p. 537.
[2] P. H. Kasai, J. Chem. Phys. **43**, 3322 (1965).
[3] J. A. Rabo *et al.*, Discuss. Faraday Soc. **41**, 328 (1966).
[4] Y. Nozue, T. Kodaira, and T. Goto, Phys. Rev. Lett. **68**, 3789 (1992).
[5] F. Blatter, K. W. Blazey, and A. M. Portis, Phys. Rev. B **44**, 2800 (1991).
[6] P. A. Anderson and P. P. Edwards, Phys. Rev. B **50**, 7155 (1994).
[7] P. P. Edwards, P. A. Anderson, and J. M. Thomas, Acc. Chem. Res. **29**, 23 (1996).
[8] L. Pauling, Z. Kristallogr. **74**, 213 (1930).
[9] Synthetic procedure for making Na_4^{3+} centers in sodalite by alkali doping is due to R. M. Barrer and J. F. Cole, J. Phys. Chem. Solids **29**, 1755 (1968).
[10] S. D. McLaughlan and D. J. Marshall, Phys. Lett. **32A**, 343 (1970).
[11] B. W. Faughnan *et al.*, Proc. IEEE **61**, 927 (1973).
[12] J. Felsche, S. Luger, and Ch. Bearlocher, Zeolites **6**, 367 (1986).
[13] V. I. Srdanov *et al.*, J. Phys. Chem. **96**, 9039 (1992).
[14] V. I. Srdanov (unpublished).
[15] The evidence for such interaction in zeolites can be found in an EPR study of B. Xu, X. Chen, and L. Kevan, J. Chem. Soc. Faraday Trans. **87**, 3157 (1991).
[16] K. G. Orrell, in *Annual Reports on NMR Spectroscopy*, edited by G. A. Webb (Academic, London, 1979), Vol. 9.
[17] G. Engelhardt *et al.*, J. Chem. Soc. Chem. Commun. **1996**, 238 (1996).
[18] H. S. Jacobsen *et al.*, Zeolites **9**, 491 (1989).
[19] H. Nakayama *et al.*, J. Am. Chem. Soc. **116**, 9777 (1994).
[20] M. E. Fisher, Philos. Mag. **7**, 1731 (1962).
[21] A. H. Morish, *The Physical Principles of Magnetism* (Wiley, New York, 1965).
[22] J. H. van Vleck, J. Phys. Radium **12**, 262 (1951).
[23] N. Blake *et al.*, J. Chem. Phys. **104**, 8721 (1996).
[24] A. Monnier *et al.*, J. Chem. Phys. **100**, 6944 (1994).